pile tip. The "Quake" term given in Table 6.1 has its origin in the soil model proposed by Smith (op cit) to describe its load deformation behaviour. In this model, it is assumed that the resistance of the soil around the pile follows a linear-elastic, then perfectly plastic load deformation path (see Figure 6.2a). The "Quake" is a measure of the deformation at the elastic limit of the "soil". In Figure 5.1 the mandrel load peak occurring at 4ms is interpreted as representing the "elastic" limit of the soil. The displacement at this time, and therefore the quake in Smith's soil model, was about 1mm.

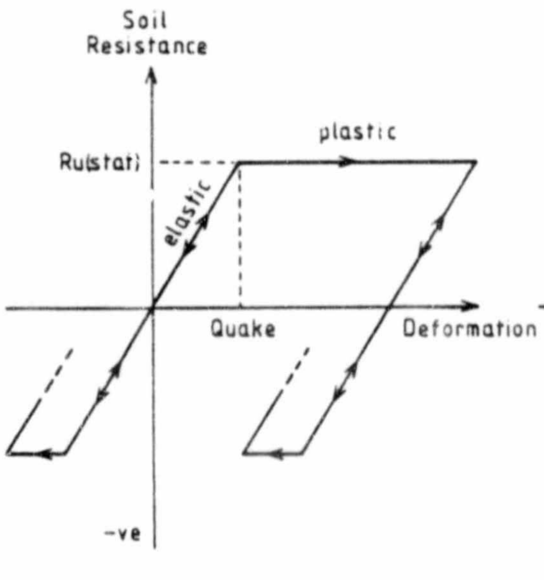

Figure 6.2a

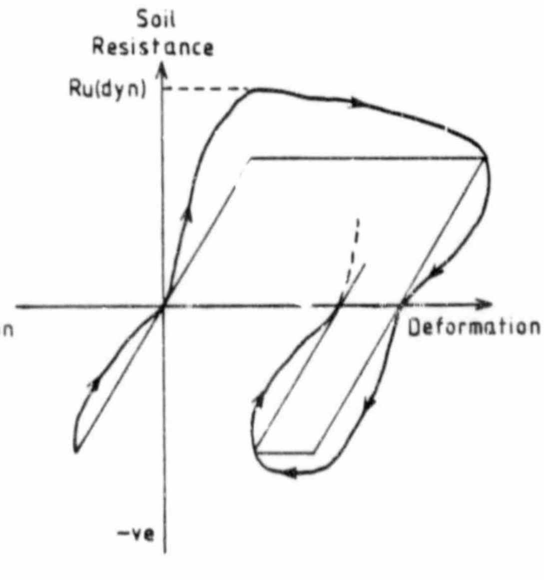

Figure 6.2b

Figure 6.2a Illustrates the soil model adopted by Smith (1960) for the wave equation analysis.

Figure 6.2b Illustrates how the inclusion of Smith's damping coefficients modify the linear elastic, perfectly plastic soil model during impact. At the pile toe, tensile loads are not permitted.

Figure 6.2 Wave equation soil model

The results of two wave equation analyses corresponding to cases 1 and 2, using the data of Table 6.1, are given in Table 6.2. A copy of a typical computer printout is given in Appendix C.

Table 6.2 : Wave Equation Analysis Results

Case No.	Ultimate static load N	Percentage load on toe	Permanent set mm	Compressive load, element No. 3, N	Tensile load Element No. 3 N
1	1306	87	7,76	2666	533
2	2612	93,5	3,57	4464	357

As can be seen in Table 6.2, the wave equation analyses for both cases 1 and 2 over-estimate the compressive load developed in the bottom pile segment (for case 2 the load of 4464N should be halved in order to compare with the model pile) and indicate that a tensile load should have been developed in the drive mandrel. The calculated pile sets for both cases also differ from the measured set. If it is considered, however, that had the model pile been circular instead of semi-circular, it would likely have penetrated less under the impact load applied than the measured 5,62mm. A tighter set would therefore have been recorded along with a higher load in the drive mandrel. It is suggested therefore that the wave equation can be used to provide a reasonable estimate of the model pile set under the given impact conditions, but that calculated mandrel loads should be treated with caution.

A major feature of Smith's version of the wave equation is that it attempts to model driven pile behaviour by simulating load transmission down a pile shaft (or drive mandrel in this case) which is approximated by a series of masses and springs. In view of the observation that the wave equation appears capable of predicting the model pile set reasonably well, it is worthwhile investigating how well transmission of a travelling stress wave describes the recorded pile behaviour.

The velocity of a stress wave in an elastic solid may be estimated from the equation:

$$V = E/\sqrt{\rho g}$$

where E is the dynamic elastic modulus of the solid and ρ is its mass density. Assuming that for the model pile (a composite of steel and silicone rubber sealant) the effective dynamic elastic modulus of the drive mandrel was approximately 200 GPa and the effective mass density was $3000 kg/m^3$, the stress wave velocity calculated according to the above equation is 8367m/s. Since the model pile was 1,32m long from the underside of the helmet to the point of the pile shoe, the time theoretically required for a stress wave to travel down the pile, be reflected at the pile toe and then reach the top of the pile again, is about 0,16ms. This corresponds to a reflection frequency of 6250Hz.

Neither the acceleration record shown in Figure 5.1, nor the oscilloscope traces of the mandrel load (at SG6) show any indication of events at frequencies of this order. Relative to the period of a reflected stress wave, impact data on the model pile recorded a sustained loading period. It can be concluded therefore that for the model pile, the influence of stress wave transmission on pile penetration behaviour during impact is slight, if not negligible. Loads in the drive mandrel, and pile head accelerations induced by impact of the drop hammer appear instead, to be influenced more by soil responses to the load than by a travelling stress wave. No physical evidence to support one of the main assumptions applied in the wave equation model was therefore identified.

Smith (1960) has noted that selection of pile lengths at between 2,44m and 3,1m provide generally satisfactory wave equation results when using the wave equation. For prototype piles where the duration of a typical impact event (20 to 50ms) causing penetration of the pile, is of a similar order of magnitude to the theoretical reflection period of a stress wave (13ms for a 30m long concrete pile), good correlations between predicted and observed pile behaviour have been found (e.g. Rausche [1972], Goble et al [1972]). This may be a criterion for the effective application of the wave equation as a design tool in the estimation of the capacity of driven preformed piles.

6.1.2 Dynamic Resistance and Pile Depth

The magnitude of the initial peak load for the shaft load data from Plates 5.1d, and 5.2b to d has been plotted against depth in Figure 6.3. These load traces include only strain gauge traces for gauges submerged in the grout. The initial peak load for SG1, with the pile toe at a depth of 450mm in Plate 5.2a, is also shown in Figure 6.3 adjusted by 230N, the amount of the load difference between SG1 and SG6 in Plate 5.1d. Although the data is sparse, there does appear to be an approximately linear trend showing increasing toe resistance with depth. It would appear therefore that dynamic resistance can be correlated with static resistance under the model pile installation conditions.

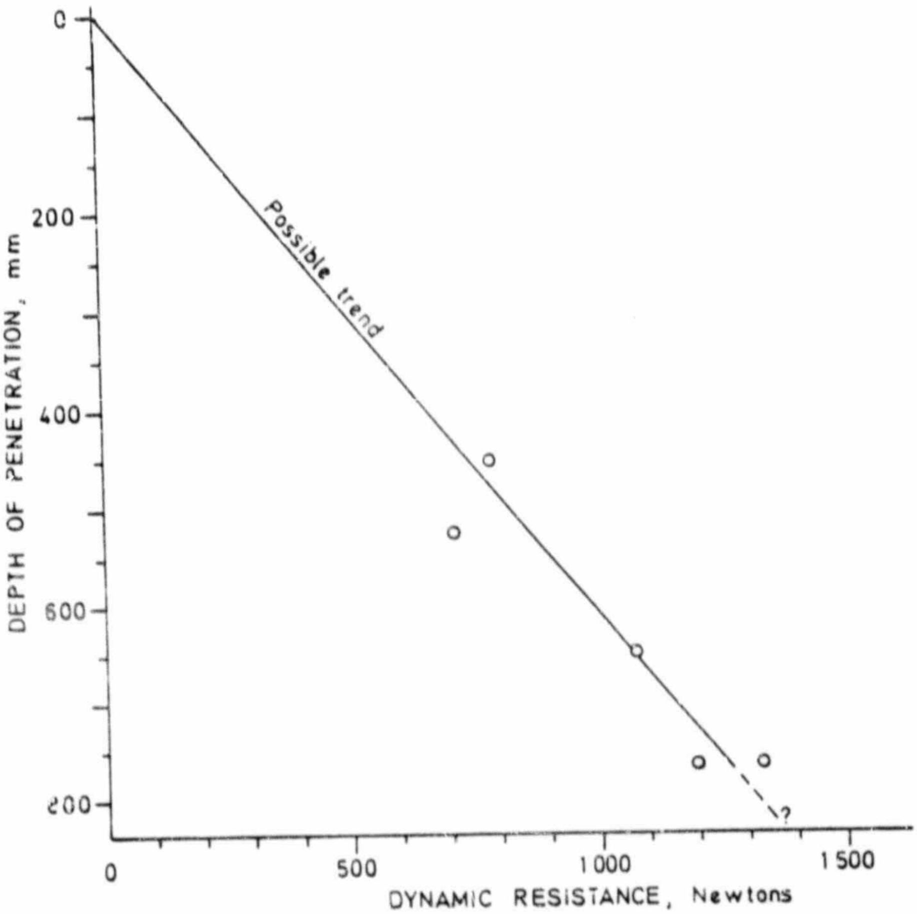

Figure 6.3 Dynamic pile resistance plotted against pile penetration depth

6.1.3 Summary

1 Load fluctuations were measured in the drive mandrel during pile installation. The reason for the fluctuations is not known, but various explanations can be considered.

2 Load response in the drive mandrel to impact varies with depth, but similar responses were observed in duplicate experiments.

3 On the scale of the model pile, the Wave Equation predicts set reasonably well, but cannot predict the loads developed in the mandrel.

4 Wave transmission as modelled by the wave equation is an unsatisfactory approximation of the behaviour of the model pile during impact.

6.2 Sand Grain Displacement Diagrams

The sand grain displacement diagrams given in Figures 5.2 to 5.5 and 5.10 to 5.17, located in the rear pocket of this volume, show, in the form of contours, the loci of sand grains subjected to equal displacements in both the X and Y directions. Measurement of the sand displacements is discussed in Appendix A. The contours mark the positions of the sand grains at the end of their respective movement increment. Figures 5.2 to 5.5 show the displacements measured during impact installation of the model pile, while Figures 5.10 to 5.17 show the displacements measured at vaious stages while load testing the pile to failure. With respect to Figures 5.2 to 5.5 the photographs of the soil around the pile toe were made between each successive impact when there was no load on the drive mandrel. These four displacement diagrams therefore record permanent shear induced sand grain displacements only. In contrast, the loads given in Tables 5.2 and 5.3 were applied to the model pile when the photographs from which Figures 5.10 to 5.17 were made. The sand grain displacement contours given in these figures therefore also include a component of recoverable elastic displacement.

6.2.1 Soil Displacements during Pile Installation

Figure 5.2 shows that horizontal displacement components (X axis) for sand grains measured on Plates 1 and 2 (Dynamic) occupy three different fields of movement. The largest, indicating outward movement away from the pile axis, occupies an egg shaped area below to the right of the pile. Most of the contours within this zone are regularly spaced and conformal.

On the line of the pile axis, and in a widening wedge about the axis below the point of the pile shoe, no horizontal movements could be detected. Along the face of the conical pile shoe, lateral displacements increased, towards the base of the inverted cone where all the contour lines converge. A second much smaller lobe shaped area, also indicating movements away from the pile, is located to the right of the shoe collar. Between this lobe and the pile shaft is an area of movement towards the pile (-ve X dispacements). The width of the zone affected by movements in this direction increases upwards from the base of the shoe cone and is evident above the top of the shoe collar.

It is clear that the sand in this area encroached into the annulus formed by the pile shoe and therefore caused a reduction in the diameter of the shaft.

The width of the measurable horizontal displacement components was about 3,1 pile diameters, measured from the pile axis. Measured from the centroid of the shoe cone, the depth to which horizontal movements was detected was about 3,2 pile diameters.

Vertical displacement components measured on Plates 1 and 2 (Dynamic) (Figure 5.3) occupy two different fields comprising a large field of downward movements of mainly large magnitude, and a smaller field of mainly small upward movements. Contours for both fields converge (as with the X displacement contours) at the base of the inverted cone pile shoe. Along the face of the pile shoe the magnitude of the vertical displacements increases downwards towards the point of the cone. Measurable vertical displacements were detected to a depth of about 4 pile diameters below the centroid of the shoe cone, but the width of the field was similar to that containing the horizontal displacement components.

The zero displacement contour separating the downward movements from the upward movements extends downwards from the base of the shoe cone at an angle of about 45° for about one and a half pile diameters and then becomes horizontal. Above this line, the upward movements become a maximum in a small area located to the right of the base of the shoe cone. Positive Y displacements have been plotted for the soil lying against the shoe collar. Despite the fact that the pile moved downwards, the soil at this interface experienced a nett upward movement.

When Figures 5.2 and 5.3 are superimposed, it can be seen that there are areas of purely horizontal and purely vertical sand movement. The largest of these is an area of purely vertical movement along the pile axis and below the pile shoe.

The accumulated soil displacements measured with respect to Plates 1 and 3 (Dynamic) are shown in Figures 5.4 and 5.5. Figure 5.4, which shows the magnitude of horizontal displacement components, is similar to Figure 5.2 in that the major soil movements are outward in a similar shaped area below and to the side of the conical pile shoe and again the contours are approximately regularly spaced and conformal. Also the maximum horizontal displacement was observed towards the base of the shoe cone. As may be expected, because the soil movements measured between Plates 1-3 (Dynamic) were caused by a pile penetration of 9,91mm (compared with 5,63mm in Figure 5.2) the displacements near the pile shoe are considerably larger than those in Figure 5.2.

The size of the movement field is also larger, 3,6 pile diameters, particularly opposite the shoe cone, where it has merged with the small lobe of outward movement seen in Figure 5.2. The depth below the pile in which outward movements were detected, however, remains similar at 3,2 pile diameters. Because of this similarity it is suggested that the outer limit of detectable permanent soil movements, corresponding to the lateral limits of the influence of the moving pile shoe on the surrounding soil at and around this depth of pile penetration, may be taken to be 3,6 pile diameters. It is not known how, or if, the width of this displacement field will change at lesser or deeper pile penetration depth.

The area in Figure 5.4 occupied by movements towards the pile axis is larger than that in Figure 5.2 and may be divided into two zones of movement. One of these zones lies against the shoe collar and has a similar shape and indicates movements of a similar magnitude to those in Figure 5.2. The other zone occupies a curved lens shaped area adjacent to the zero displacement contour separating the two movement fields.

Apart from the magnitude of the movements they record, the pattern of vertical displacement component contours shown in Figure 5.5 is very similar to that of Figure 5.3. Upward and downward movement fields occur in similar regions on the diagrams and occupy similar areas. It appears that the limit of detectable vertical soil movements below the pile toe in Figure 5.5 has moved downwards approximately in unison with the point of the pile shoe.

As with Figures 5.2 and 5.3, comparison of Figures 5.4 and 5.5 also show areas of purely horizontal or purely vertical movement. The major zone of purely vertical movement is again located in a wedge shaped area along and to the side of the pile axis below the point of the pile shoe. A significant area of purely horizontal movement is apparent opposite the shoe cone.

The 5,63mm vertical downward movement of the pile shoe in Figures 5.2 and 5.3 corresponds to a movement of 4750 plotter units. In Figures 5.4 and 5.5 the pile movement of 9,91mm expressed in plotter units is 8375 units. It has been noted in Appendix A that for various reasons, not all possible contours have been drawn in areas of high displacement gradients such as that bordering the pile shoe. It is clear from Figures 5.3 and 5.5, however, that the vertical displacement component of sand grains lying close to the conical pile shoe is significantly less than the displacement of the shoe itself. There was therefore differential movement between the pile and the surrounding soil which must have imposed frictional restraints on displacement of the pile. It was not possible in the photographs of the soil movements obtained in this project to identify precisely the nature of the movement of the soil past the pile shoe. Because, however, most identifiable sand grains near the pile shoe remained in similar positions to each other between each incremental displacement of the pile, it is suggested that pile penetration was associated mainly with sliding rather than rolling of sand grains against the interface.

Figures 6.9 and 6.15, which are discussed further in section 6.4, show that the trajectories of displaced sand grains lying close to the conical face of the pile shoe were oriented at an angle measured counter-clockwise from the pile axis of about 30° near the point of the shoe to about 50° near the base of the cone. Using these trajectory angles, and knowing the displacement of the pile shoe, possible horizontal and vertical displacement components of sand grains lying in contact with the shoe/soil interface at the start, and at the end of a displacement increment, can be calculated using the geometrical relationships shown in Figure 6.4. Table 6.3 lists the calculated displacements.

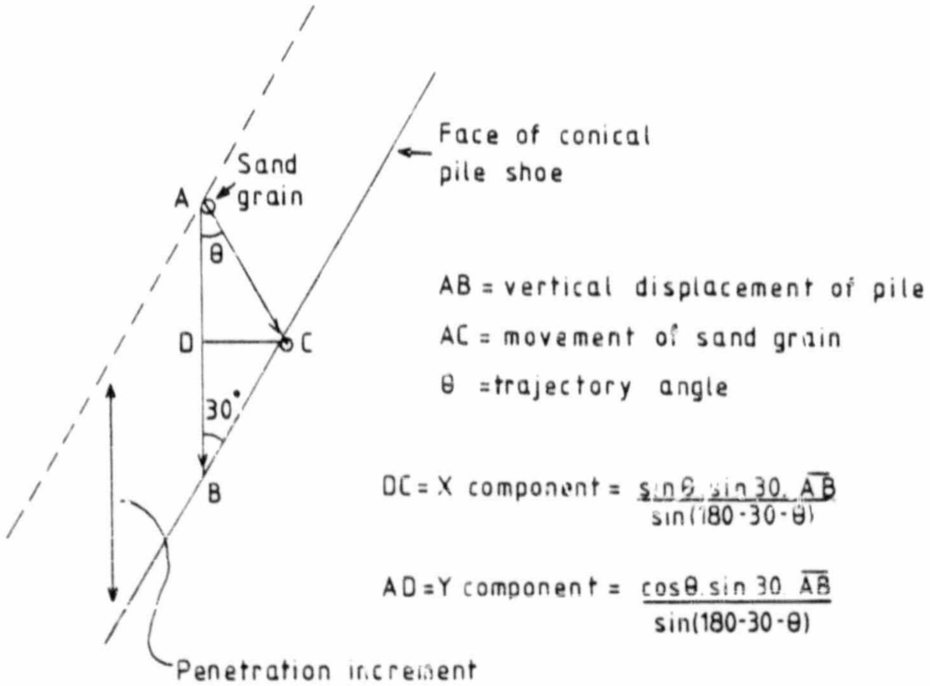

Figure 6.4 Sketch showing displacement of a sand grain remaining in contact with the pile shoe, and calculation of its displacement components.

Table 6.3 : Calculated displacement components for sand grains lying in contact with the pile shoe during impact penetration.

Displacement of Pile Shoe mm	Trajectory Angle	X Component Plotter Units	Y Component Plotter Units	Slip Plotter Units
5,63m(4750)	30° (point)	1371	2375	2742
	50° (base)	1347	1550	3695
9,91mm(8375)	30° (point)	2418	4188	4835
	50° (base)	3257	2733	6515

The dimension BC in Figure 6.4 indicates the amount of slip along the shoe/soil interface experienced by the sand grain. This has also been calculated and is listed in Table 6.3.

Comparison of the data in Table 6.3 with the contour diagrams (Figures 5.2 to 5.5) shows that there is reasonable agreement between the contours drawn and the calculated displacements for horizontal movements away from the point of the shoe cone. Near the point of the shoe, agreement is poor, however. As discussed in Appendix A, section A.5, there may be local effects due to an inability of the model pile system to simulate true axial symmetry, in the area around the point of the pile shoe. This may explain the apparent anomaly in the displacement diagrams as drawn.

With regard to the vertical movement components, the contours shown in Figure 5.3 show reasonable agreement with the data in Table 6.3, but the contours shown in Figure 5.5 show poor agreement near the point of the pile shoe. The local effects mentioned above concerning horizontal movements may also apply to the vertical movements.

6.2.2 Soil Displacements during Static Load Testing

The sand grain displacement diagrams obtained during static loading of the model pile and given in Figures 5.10 to 5.17 show a number of different features when compared to the diagrams showing impact installation effects. The major differences are probably caused by the presence of a solid shaft (as compared to a liquid grout column) located above the pile shoe. Pile toe movements associated with the displacement diagrams were also significantly smaller than those from which the impact installation diagrams were drawn, and progressive displacements, with widening of the observed displacement fields, can be clearly seen. Most of the measured vertical displacement components were downwards and most of the horizontal movements were observed to be outwards from the pile axis.

All the diagrams can be divided into four zones showing similar features. These include:

(a) A bulb shaped area associated with movements around the shoe cone. Contours converge to the base of the inverted cone shoe, but some of the contours are continuous into the next section.

(b) Adjacent to the shoe collar, contours tend to converge. This is particularly noticeable with the vertical sand movements.

(c) Above the shoe collar is a zone against the pile shaft which includes two areas of horizontal movement and increasing vertical movements away from the pile shoe. The separation between the two horizontal movement fields occurs at about 50mm above the shoe collar where the width of the vertical movement field starts to widen.

Plate 5.3d, which shows a portion of the pile shaft above the top of the shoe collar, reveals the presence of a slight narrowing on the pile shaft at about 45mm from where the top of the shoe collar was located. The collection of impact installation data began when the shoe collar was located approximately at this position. During this period the impact rate dropped considerably and, at the end of it, the reaction beam arrangement was placed in position to measure the pile toe load before the grout shaft cured and hardened against the surrounding soil. It seems likely that the slight necking at this position was a consequence of these activities and that the presence of this neck has had a profound effect on the measured soil displacements.

(d) The fourth zone of movements refers to small scale perimeter movements. Although clearly defined as a zone of small upward movements in the vertical displacement diagrams (Figures 5.13, 5.15 and 5.17), the perimeter zone associated with horizontal movements is irregular and patchy, and progressive movements are less easy to identify.

Horizontal movements were detected over a width of between 3 (Figure 5.10) and 3,6 (Figures 5.12, 5.14 and 5.16) pile diameters from the pile axis. It is not certain that the small scale outward and inward movements shown beyond the 25 unit contour in Figure 5.10 are meaningful. It is considered that the boundary of the X displacements in this diagram should lie close to and approximately follow the 25 unit contour. On this basis, Figure 5.10 differs considerably from the other horizontal displacement diagrams.

The width of the displacement field is approximately constant from about the level of the point of the pile shoe upwards though there is an indication that it may narrow at shallower depths. Measured from the centroid of the shoe cone, the movement field extends to about 1,9 pile diameters below the pile (Figure 5.10) increasing at a total shoe movement of 6,33mm to about 2,5 pile diameters below the pile. Within the movement zone associated with the pile shoe, a patch of peak movements can be seen located in an area offset from, but close to, the shoe itself.

Table 6.4 which is similar to Table 6.3 presents calculated displacement components for sand particles which may have remained in contact with the edge of the shoe during a movement increment. The displacement trajectory angles in Table 6.4 for sand grains lying close to the shoe face, were obtained from the relevant principal strain direction diagrams (Figures 6.22, 6.28, 6.34, 6.40). It is clear from this table that the plotted and calculated horizontal displacement data agree closely away from the point of the shoe cone where the higher movements were recorded. Agreement between calculated and measured displacements near the point of the shoe is, however, not good. Following the discussion in Appendix A, section A.5, it is suggested that due to the high curvature of the conical shoe towards the apex of the cone, axial symmetry conditions were disturbed, and the displacement data obtained may be mainly due to local effects.

Adjacent to the pile shaft. progressive increases in horizontal displacement with increasing toe movement are clearly shown in Figures 5.10, 5.12, 5.14 and 5.16. Although the contours have been drawn in contact with the pile shaft suggesting that the soil is progressively detaching itself from the shaft, this is unlikely to have occurred in practice. Details of the boundary layer movements were not identified during the grain co-ordinate measurements, mainly because at the scale of the displacement photographs there was insufficient clarity in the images to resolve the large displacements which occurred. It may be assumed that, due to the roughness of the pile shaft with asperities at least of the order of the sand grain diameters, the soil movements in the boundary layer were complex.

Apart from Figure 5.11, the vertical displacement component diagrams show similar and progressive features (Figures 5.13, 5.15 and 5.17). These include a large region of small upward movements. Opposite the shoe collar, roughly parallel displacement contours adjacent to the pile shaft extend outwards to about 3 pile diameters from the pile axis and a large lobe shaped area of downward movements extends to between 2,75 and 3,0 pile diameters below the centroid of the shoe cone.

In Figure 5.11, however, the width of measurable vertical movements is shown as at most 2,0 pile diameters from the pile axis and no upward movements were recorded.

Comparison of the displacement contour diagrams for Plates 1-4 static (Figures 5.14 and 5.15, submerged test), and Plates 1-5 static (Figures 5.16 and 5.17, drained test), indicates that there are some areas in which the soil movements either remained unchanged or reversed in direction during the drained test relative to the submerged test. In general, the changes in the progressive movement trends are of a sufficiently small magnitude to be explained in terms of measurement and/or contour plotting error. They may, however, also be indicative of the effect of increasing the overburden pressure by draining off the water in the sand box.

The data in Table 6.4 gives calculated components of vertical displacement for the movement of theoretical sand grains lying in contact at two positions with the inclined face of the shoe cone during a displacement increment. Most of this data agrees well with the contour diagrams.

When associated pairs of the horizontal and vertical displacement diagrams are superimposed, zones of purely vertical movement can be seen to have occurred near the pile axis towards the perimeter of the vertical displacement field. Purely horizontal movements occurred in a narrow strip parallel to the pile axis and beyond the perimeter of the vertical mc [illegible] eld.

Table 6.4 : Calculated displacement components for sand grains lying against the pile shoe during static loading

Displacement of Pile Shoe mm	Trajectory Angle	X Component Plotter Units	Y Component Plotter Units	Slip Plotter Units
0,83mm (704)	19°	152	441	304
	40°	241	287	482
2,00mm (1687)	25°	435	933	470
	35°	534	762	1068
4,85mm (4095)	25°	1056	2265	2112
	26°	1083	2220	2166
6,33mm (5342)	27°	1446	2838	2892
	32°	1603	2565	3206

No significant differences could be detected between the displacement diagrams showing observed soil movements during the test in submerged sand (Figures 5.10 to 5.15), and Figures 5.16 and 5.17 showing movements observed during the test in drained sand.

6.2.3 Summary

1 At the depth at which soil displacement measurements were made during pile installation (L/d = 12,5), the width of the measurable displacement field extended laterally from the pile axis to about 3,6 pile diameters, and down to a depth of about 4 pile diameters below the centroid of the shoe cone. Movements occurred in all directions, though mainly downwards and outwards.

2 Axial symmetry conditions in the semi-circular model pile may not be correctly simulated near the point of the pile shoe.

3 The patterns of soil displacements associated with impact installation differed from those associated with static loading at similar toe displacement.

4 The presence of a slight neck in the pile shaft about 1,5 pile diameters above the shoe cone had a profound effect on the observed soil movements.

5 The width of the soil movement field during static load testing was about 3,6 pile diameters (the same as during impact) to the side of the pile axis and extended to about 2,5 pile diameters below the centroid of the shoe cone.

6 During static loading all horizontal movement components were outwards and most vertical movements were downwards.

6.3 Discussion of Static Load Tests

Load/settlement data for the static load tests carried out under both submerged and drained soil conditions have been given in Figures 5.6 to 5.9 (pages 5.18 to 5.22) and Tables 5.2 and 5.3 (pages 5.23). Both these tests were carried out to pile failure defined as plunging of the load/settlement curve when the pile continued to move downwards with no increase in load capacity. The records include load distribution down the pile shaft and estimated toe load at all stages of loading, as well as elastic rebound of the pile under no load conditions on termination of the test cycles. Residual loads measured after a rest period following each load increment are assumed to reflect the strength of the sand under effective stress conditions. "Apparent cohesion" is therefore ignored.

6.3.1 Comparison of Submerged and Drained Test Results

It should be recalled that the load test carried out in drained sand was effectively a continuation of that done in submerged soil conditions. Sand around both the pile shaft and pile toe had already been sheared to a residual strength state during the first static load test.

Figure 5.6 shows the main features of the two static load test results. The differences between these two load/settlement cycles may be listed as follows:

1 A pile head settlement of 3,63mm (L4) was required to achieve the ultimate load on the pile in submerged sand, while 2,90mm (L10) was required in drained sand. The respective residual ultimate pile loads were about 3082N (L5) and 4123N (L11) at failure.

The residual pile load after the L4 load increment during the test in submerged sand was 3198N which was greater than the residual pile load remaining after the L5 increment. Figure 5.7 (submerged sand test) shows that the rest period during which load on the pile was maintained following the L5 increment, was considerably longer than the L4 rest period. It is likely that soil creep, with corresponding load adjustment, occurred during the sustained L5 rest period. Had a similar sustained rest period been permitted following L4, a similar residual load may have been recorded.

2 Although minor increases in toe load continued to occur after the L2 load increment in the submerged sand test, the ultimate toe load projected from SG1 in Figure 5.8 of about 970N was achieved at a pile head movement of 1,06mm (L2). During the test, in drained soil conditions, the ultimate toe load projected from SG1 in Figure 5.9 of about 1350N (L11) was not achieved until the pile head had moved 3,65mm. Close examination of the load/settlement curve for SG1 shown in Figure 5.6 suggests that the toe load may have continued to increase slowly with further pile penetration. The rest period allowed after the application of the L11 load step was relatively short compared to that following L5 in the submerged sand test. Had the rest period after L11 in the drained sand test been extended, it is possible that the residual load on the pile toe would have been less than 1350N. When the toe load reduction measured during the submerged test is extrapolated to the drained test, the estimated ultimate toe load under drained conditions becomes 1270N. It is suggested that this is a more realistic estimate

than 1350N and has been adopted as the ultimate toe load in subsequent discussions. A major portion of this ultimate load had, however, been developed after a head movement of 1,16mm (L7). If the glass front panel/pile friction corrections described in Appendix E are applied to the estimated toe loads, the ultimate bearing capacity of the pile toe in submerged sand becomes 854N and in drained sand 1118N. Expressed as an average end bearing pressure on the cross-sectional area of the hemispherical pile shoe, the ultimate toe capacities were 604 kPa and 791 kPa respectively.

3 During the submerged sand test, shaft friction load continued to increase, albeit slowly, for some 2,5mm of additional head movement after the ultimate toe load had been achieved. During the test in drained sand, shaft friction continued to develop until the pile head had moved 2,9mm (L10).

6.3.2 Comparison of Submerged and Post-Installation Load Test Results

The rest load measured on the pile toe during the immediate post-installation load test on the model pile, was 1138N. This differs significantly from the rest load of about 970N measured at failure of the pile during the load test in submerged sand. Even if allowance is made for friction along the glass panel as discussed in Appendix E, the adjusted loads becoming 957N and 854N respectively, the difference in the measured toe loads remains significant. The lower ultimate toe load measured during the latter static load test suggests that different failure mechanisms around the pile toe are applicable to piles with a solid shaft and piles with a fluid grout shaft. The limiting vertical stress on the cross-sectional area of the pile toe during the immediate post-installation static load test was 677 kPa.

6.3.3 Shaft Friction Capacity

Figures 5.8 and 5.9 show the measured load distribution down the pile shaft for the various load increments. In both these diagrams, the load difference between SG4 located in the thickened portion of the shaft and SG5 located above the grouted shaft, follows a similar trend. Initially, at L1 in Figure 5.8 and L.3 in Figure 5.9, the difference was small. The pile head movement at these two load increments were similar at 0,23mm and 0,25mm. With greater pile head movement, the difference increased reaching approximately constant values at L3 in the submerged sand test, and at L9 in the drained sand test. The pile head movements corresponding to these load increments were again similar at 2,24mm and 2,31mm respectively.

Because removal of the grout reservoir after installation of the pile was completed would have left an annulus of loose to very loose sand around this portion of the shaft, it is thought that some of the load shedding that occurred between SG5 and SG4 was caused by the lower face of this collar bearing on the underlying soil, rather than by pile/soil friction. The balance of the load shed between SG5 and SG4 was probably by friction with the glass panel.

Elsewhere along the pile shaft, load differences recorded between the strain gauge groups were due to load shedding into the soil through shear along the pile shaft and friction with the glass front panel. Average shear stresses have been estimated for the pile/soil friction at the mid-points between adjacent strain gauge groups. Tables 6.5 and 6.6 list the calculated skin friction stresses which are plotted in Figures 6.5 and 6.6. The stresses have been calculated using the residual load data in Tables 5.2 and 5.3, the measured pile diameters given in Section 5.2, and by applying the glass/pile friction corrections described in Appendix E. At the bottom of the pile the friction stress has been calculated along that part of the shaft between SG1 and the bottom of the shoe collar. It therefore includes the friction stress for metal to soil contact along the collar as wide as grout to soil contact above the collar.

Table 6.5 : Measured (), and corrected shear stresses at mid-points of strain gauge groups. Load test in submerged sand.

Load Step No.	SG4/SG3	SHEAR STRESSES kPa SG3/SG2	SG2/SG1	SG1/Toe
L1	(18) 11	(34) 26	(17) 12	(9) 7
L2	(22) 13	(38) 29	(20) 15	(10) 7
L3	(22) 13	(44) 33	(30) 22	(8) 6
L4	(21) 13	(51) 38	(33) 24	(8) 6
L5	(21) 13	(53) 40	(30) 22	(6) 5

(Weighted average corrected shear stress along shaft for L4 = 23,3 kPa.)

Table 6.6 : Measured () and corrected shear stresses at mid-points of strain gauge groups. Load test in drained sand.

Load Step No.	SG4/SG3	SHEAR STRESSES kPa SG3/SG2	SG2/SG1	SG1/Toe
L1	(16) 9	(21) 16	(18) 14	(11) 8
L2	(23) 14	(35) 26	(27) 20	(18) 13
L3	(28) 17	(45) 34	(34) 25	(24) 17
L4	(32) 19	(52) 39	(39) 28	(24) 17
L5	(29) 18	(54) 40	(40) 30	(23) 16
L6	(30) 18	(56) 42	(41) 30	(22) 16
L7	(31) 18	(57) 43	(41) 30	(22) 16
L8	(31) 19	(59) 44	(40) 29	(19) 14
L9	(30) 18	(60) 45	(40) 29	(18) 13
L10	(32) 19	(61) 46	(37) 27	(18) 13
L11	(29) 17	(62) 46	(38) 27	(18) 13

(Weighted average corrected shear stress along shaft for L8 = 29,8 kPa)

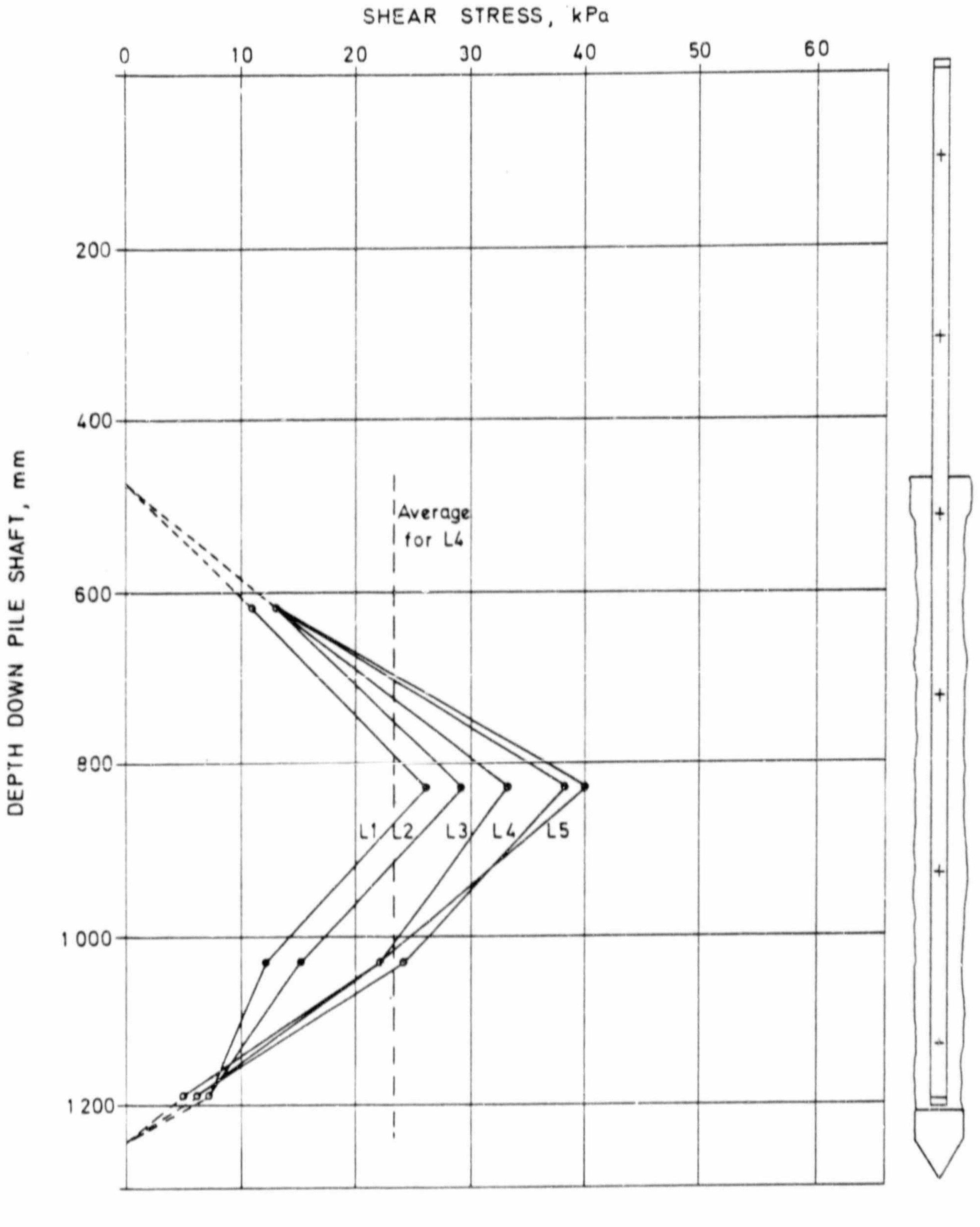

FIGURE 6.5 Shear stress distribution down the pile shaft during the load test in submerged sand

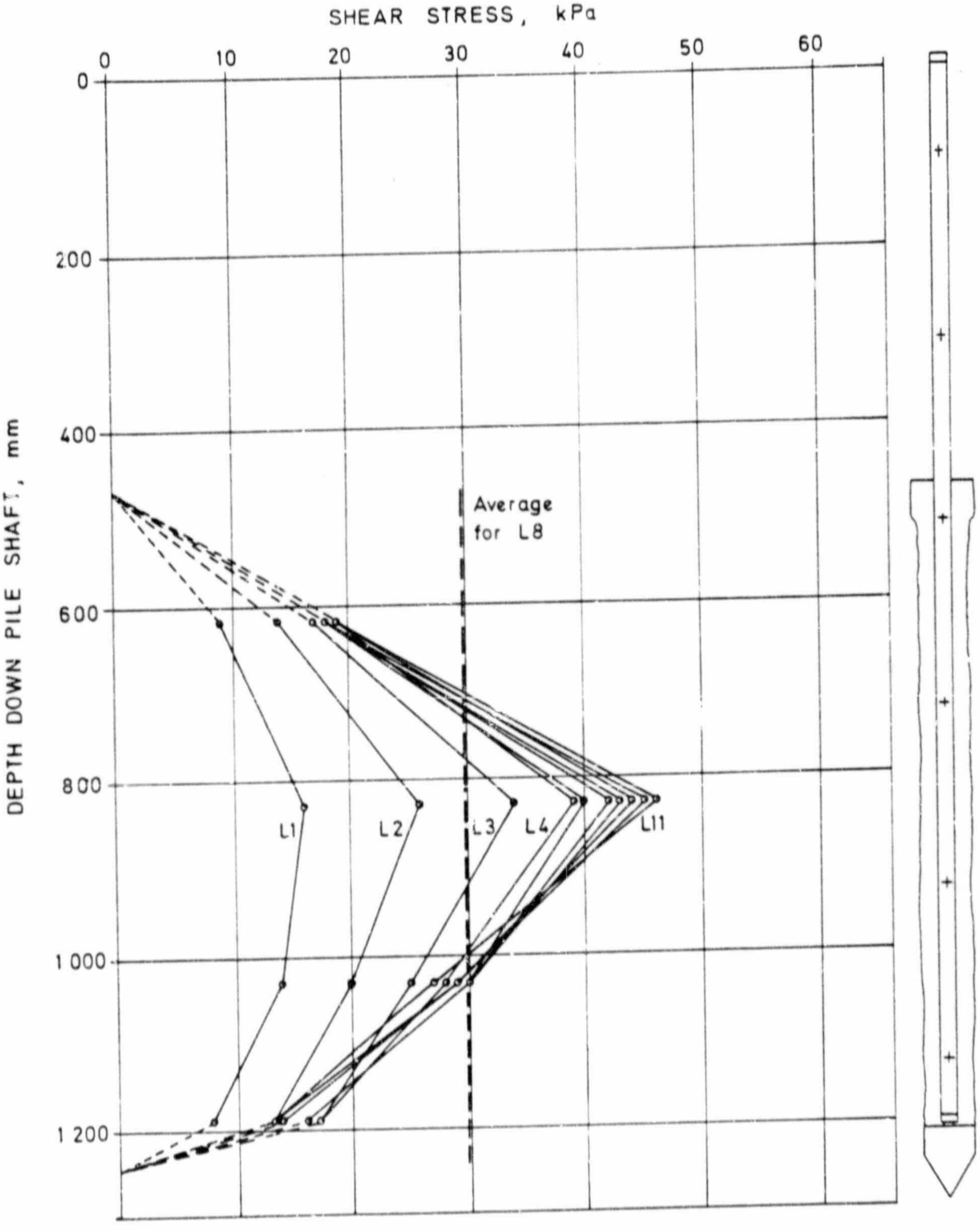

FIGURE 6.6 Shear stress distribution down the pile shaft during the load test in drained sand

The data in Table 6.5 and Figure 6.5 indicate that the shear stress distribution down the pile shaft during the load test in submerged sand was approximately triangular. This pattern was duplicated in the drained sand test at pile head displacements in excess of 0,25mm (L3, similar to L1 at 0,23mm in the submerged test). Apart from small fluctuations, the developed shear stresses increased progressively with each incremental load step and then decreased except over the portion of pile shaft between SG2 and SG3 where no decrease was recorded. Over this portion of the shaft, it appears that the ultimate skin friction capacity of the shaft did not develop. The measured skin friction was, however, probably very close to the ultimate.

6.3.4 Elastic Recovery at End of Static Load Tests

Table 5.2 records that the elastic recovery measured at the pile head after removal of load at the end of the load test carried out in submerged sand (between L5 and L6) was 0,26mm while that for the test in drained sand, Table 5.3, (between L11 and L12) was 0,34mm. From the known stiffness of the drive mandrel (measured by the strain gauges) and the measured elastic modulus of the hardened grout, it is estimated that of these recoveries, 0,093mm and 0,125mm respectively, were due to elastic rebound of the pile shaft itself. Rebound of the loaded soil at the end of the two load tests, therefore, amounted to 0,17mm for the test in submerged sand and 0,22mm for the test in drained sand. Expressed in terms of plotter units as given in the displacement diagrams, these recoveries correspond to 200 units and 260 units.

The ratio of the estimated ultimate toe capacities obtained for the loaded pile in submerged and drained sand is:

$$970/1270 = 0{,}764$$

The ratio of the corresponding elastic recoveries is:

$$200/260 = 0{,}769$$

The similarity of these ratios suggests a linear correspondence and therefore that the elasticity of the soil mass affecting pile rebound was similar in both tests.

Tables 5.2 and 5.3 both record the existence of tensile loads developed at SG1 and SG2 after removal of load at the pile head. The development of such residual loads in piles subject to fluctuating loads is well known (eg Hunter and Davisson [1969], Vesic [1977], Coyle and Castello [1981], O'Neill et al [1982]). In most cases, the residual load remaining in the lower portion of a long slender pile is compressive due to the soil at the top of the pile resisting rebound of the pile shaft. The tensile loads developed during this experiment may be due to the elastic moduli of the pile and the soil being significantly different, the pile being more stiff than the soil (as shown by the rebound of the pile toe). On removal of the applied load, the soil surrounding the pile may have attempted to rebound more than the pile, with the result that a tensile load developed near the toe of the pile.

6.3.5 Submerged and Drained Test Sand Capacities

The ultimate bearing capacity of the sand at the pile toe has been given in 6.3.1 (2) as 604 kPa for the submerged load test, qb (sub), and as 791 kPa for the "drained" load test, qb (drain). Tables 6.5 and 6.6 give the average shear stresses along the length of the pile shafts as 23,3 kPa (fs [sub]) and 29,8 kPa (fs [drain]) for the submerged and "drained" tests respectively.

The overburden pressure, qv, during the "drained" test should have been greater than the submerged test by an amount equal to the effective unit weights of the soil applicable to each test; ie:

$$\gamma'(\text{drain})/\gamma'(\text{sub}) = 17{,}49/6{,}73 = 2{,}6$$

For an homogenous soil deposit, and using equations (2-2) and (2-3), fs and qb are proportional to qv, and it is reasonable to expect that for the model test results, drained values of fs and qb should be greater by 2,6 times than the submerged values. This was clearly not so, as,

$$qb\ (drain)/qb\ (sub) = 791/604 = 1{,}31$$

and

$$fs(drain)/fs(sub) = 29{,}8/23{,}3 = 1{,}28$$

Because of the similarity in the magnitude of these ratios, it would appear that a uniform change in lateral stress conditions occurred as a result of draining the sand box throughout the soil mass, influencing the pile capacity. For this reason the drained test results are not directly comparable to the submerged test results.

6.3.6 Summary

1 Greater pile head movement (3,65mm) was required to mobilise the ultimate pile resistance (3082N) in submerged soil conditions than in drained conditions (2,90mm and 4123N). Greater head movement (3,65mm) was, however, required to mobilise full toe resistance in the drained soil than in the submerged soil (1,06mm). Ultimate shaft loads in both tests developed at similar pile head movements.

2 The pile toe load measured immediately after installation of the pile before the grout cured (1138N) was greater than the estimated toe load (970N) developed during the static test in submerged sand. The estimated ultimate toe load for the static test in drained sand was 1270N. When proposed corrections for friction on the glass front panel are applied to these toe loads, the corrected loads become 957N, 854N and 1118N respectively.

3 The magnitude of the estimated shear stresses developed between the pile shaft and the soil in both static load tests followed a triangular shape.

4 A tensile load developed in the lower portion of the pile shaft after removal of all applied loads at the end of both static load tests.

5 Stress relief probably occurred when draining the sand box of water prior to conducting the "drained" static load test. The pile loads measured during this test are therefore not directly comparable to those obtained during the submerged test.